International Journal of Heat and Mass Transfer xxx (2018) xxx–xxx

Contents lists available at ScienceDirect

International Journal of Heat and Mass Transfer

journal homepage: www.elsevier.com/locate/ijhmt

Heat transfer during condensing droplet coalescence

Sanjay Adhikari, Alexander S. Rattner *

Department of Mechanical and Nuclear Engineering, The Pennsylvania State University, University Park, PA 16802, United States

ARTICLE INFO

Article history:
Received 26 February 2018
Received in revised form 3 May 2018
Accepted 2 July 2018
Available online xxxx

Keywords:
Dropwise condensation
Volume of Fluid (VOF)
Coalescence

ABSTRACT

Dropwise condensation can yield heat fluxes up to an order of magnitude higher than filmwise condensation. Coalescence is the primary mode of growth for condensing droplets above a small threshold size (*e.g.*, radius $r > 2$ μm for water at 1 atm), but no prior studies have quantitatively assessed heat transfer during coalescence. Previous models of dropwise condensation have generally described coalescence as an instantaneous event, with a step reduction in heat transfer rate. However, coalescence and recovery of a quasi-steady droplet temperature profile requires a finite time, during which the direct droplet condensation heat transfer rate gradually decays. Additionally, during this period, the droplet may oscillate, repeatedly clearing the surrounding surface and resulting in high overall heat fluxes. This study employs Volume-of-Fluid (VOF) simulations to quantitatively assess these two transient heat transfer processes during droplet coalescence. It is shown that the direct mechanism of gradual heat transfer decay can be represented by a decaying exponential function with a time constant τ. Simulations are performed to determine $\tau(r_1, Rt)$ for $(1\ \mu m \leqslant r_1 \leqslant 25\ \mu m;\ 1 \leqslant Rt \leqslant 4)$ where r_1 is the radius of the smaller droplet and Rt is the radius ratio between the two merging droplets. For water at atmospheric pressure this spans the range of droplet sizes through which most of the heat transfer occurs on a surface ($\sim 80\%$). A simple correlation is proposed for $\tau(r_1, Rt)$ for the studied droplet size range, fluid properties, and surface conditions. These simulations are also employed to determine the order of magnitude of heat transfer enhancement due to repeated clearing of the surrounding surface as droplets coalesce. Findings can inform improved models of dropwise condensation that more accurately predict transient heat transfer during coalescence events.

1. Introduction

Dropwise condensation is a promising high-flux heat transfer mechanism with applications in power generation [1], desalination [2], and power electronics thermal management [3]. Dropwise condensation heat fluxes can be an order of magnitude greater than in filmwise condensation [4,5]. The dropwise condensation process initiates at discrete nucleation sites, which are distributed over a cooled surface [6]. Droplets larger than the smallest thermodynamically viable droplet [7] grow by condensation and coalescence with neighboring droplets until they are large enough to be removed by body forces. Sliding, merging, and removal of droplets exposes portions of the cooled surface on which new droplets can nucleate, allowing the dropwise condensation process to continue in a cyclic steady-state fashion [8].

Beysens and Knobler [9] described three regimes of dropwise condensation with a 100% relative humidity nitrogen-steam mixture flowing over a cooled surface (vapor temperature $T_V = 23\ ^\circ C$; surface temperature $T_S = 21\ ^\circ C$). Initially, in the first regime, for $t \leqslant 1$ s, a surface is covered by a homogenous pattern of small droplets with both r and a smaller than 2 μm (here t is time, r is the radius of a droplet and a is the distance between two droplets). The droplets primarily grow by direct condensation [10]. In the second regime, for $1 \leqslant t \leqslant 300$ s and $2 < r \leqslant 300$ μm, the droplets primarily grow due to coalescence. In the third regime, $t > 300$ s, the droplet size distribution on the surface reaches a statistically steady state condition, with equilibrium rates of droplet removal, production, and growth. Their finding suggests that coalescence is the dominant mode of growth for ambient pressure water droplets with $r > 2$ μm. Following the size distribution model of Graham and Griffith [6] such droplets would account for 60–70% of the surface coverage during dropwise condensation, indicating the importance of understanding the coalescence process.

A number of recent studies have investigated the details of droplet coalescence during dropwise condensation. Chu et al. [11] have studied the effect of surface wettability and contact angle hysteresis on droplet coalescence. Sprittles et al. [12,13] have developed a finite element framework, which considers formation

* Corresponding author at: 236A Reber Building, University Park, PA 16802, United States.
E-mail address: Alex.Rattner@psu.edu (A.S. Rattner).

https://doi.org/10.1016/j.ijheatmasstransfer.2018.07.005
0017-9310/

and then gradual disappearance of an internal interface, to study the coalescence of two merging droplets. Their numerical framework was also used by Enright et al. [14] to model coalescence induced jumping of droplets on ultra-low adhesion surfaces. Enright et al. [14] also validated their findings experimentally. Chen et al. [15] have also conducted experiments on superhydrophobic surfaces with hierarchical microscale/nanoscale roughness to study coalescence induced jumping of droplets.

While many such investigations have advanced understanding of droplet coalescence hydrodynamics [11–25], limited information is available on heat transfer during coalescence. Numerical simulations have been conducted of the overall dropwise condensation process, tracking growth of individual (ideal hemispherical) droplets in a Lagrangian sense [26,27]. In these studies, the heat transfer rate of individual droplets has been modeled in a quasi-steady function (independent of droplet history), with heat transfer rates depending on current droplet radius, fluid properties, and operating conditions (surface temperature and saturation temperature) [18]. Such studies have modeled coalescence as an instantaneous event [26–28]. Typically, in these models, when two parent droplets overlap at the end of a simulation time-step, they are replaced with a single larger hemispherical child droplet (volume conserved) with its center at the volume-weighted mean of the parent droplet centers. At the next simulation time-step, the heat transfer rate of the larger droplet corresponds to the quasi-steady value for its size. However, the actual droplet coalescence proceeds over a finite time interval, and the resulting child droplet requires a period of time to recover the quasi-steady temperature profile and heat transfer rate. Additionally, these models do not predict the unsteady hydrodynamics of coalescence. Actual droplets can have complex time varying shapes during coalescence, and the heat transfer rate depends on the shape of the droplet base [29]. Moreover, coalescing droplets oscillate and sweep the area around them, repeatedly re-initializing nucleation on the surrounding surface, and potentially increasing the overall heat transfer rate.

It is not yet known what role coalescing droplet transient heat transfer and hydrodynamics have on the overall dropwise condensation process. Fig. 1 shows a representative time series of the coalescence process with two droplets of equal radii (25 μm), obtained using the interface tracking (Volume of Fluid – VOF) simulation approach method presented later in this paper. This study seeks to provide initial quantitative data on droplet coalescence heat transfer to inform improved models of dropwise condensation.

Considering the simplified coalescence assumption of prior modeling studies of dropwise condensation, the present study seeks to:

(1) Perform interface resolving simulations of droplet coalescence to identify heat transfer trends and timescales
(2) Determine the extent to which the instantaneous coalescence assumption under-predicts condensing droplet heat transfer rates
(3) Formulate an analytic model for time-dependent heat transfer after droplet coalescence, which could be incorporated into Lagrangian simulations of dropwise condensation to improve heat transfer predictions
(4) Estimate the degree of heat transfer enhancement due to repeated clearing of droplets from the surrounding wall area by oscillating coalescing droplets

To achieve these goals, this study performs Volume-of-Fluid (VOF) simulations of coalescence of pairs of water droplets in saturated steam environment at 100 kPa on a previously characterized surface (hydrophobic silane). The VOF approach is validated using hydrodynamic data from the literature [30] and a set of conduction-only Finite Element (FEM) heat transfer simulations (based on the approach given by Adhikari et al. [31]). A parametric study is performed for varying droplet radii ($r \in [1, 100]$ μm – most of the heat ~80% is transferred through this range of droplet sizes [32]) and varying ratios of the merging droplet radii ($\mathrm{Rt} \in [1, 4]$). It is shown that transient condensation heat transfer during coalescence can represented by an exponential curve with time constant τ. A simple correlation is proposed for τ for the range of conditions in this parametric study. A representative coalescence case is simulated with a subgrid scale model to estimate the heat transfer enhancement due to an oscillating droplet repeatedly clearing surrounding microscopic droplets.

2. Modeling approach

2.1. Governing equations

This study employs the Volume of Fluid (VOF) interface tracking formulation, as implemented in OpenFOAM® [33]. VOF is an interface capturing technique in which the liquid volume fraction in each computational cell is represented by a scalar field $\phi \in [0, 1]$ ($\phi = 0$ all vapor in cell, $\phi = 1$ all liquid in cell), and a single set of governing mass, momentum, and thermal energy transport equations is solved for both phases. The phase fraction field is advected by the solved velocity field (Eq. (1)). Fluid material properties at each point are determined as a ϕ-weighted average of liquid and vapor values (Eqs. (2) and (3)).

$$\frac{\partial \phi}{\partial t} + \frac{\partial}{\partial x_i}(u_i \phi) = \dot{\phi}_{pc} \tag{1}$$

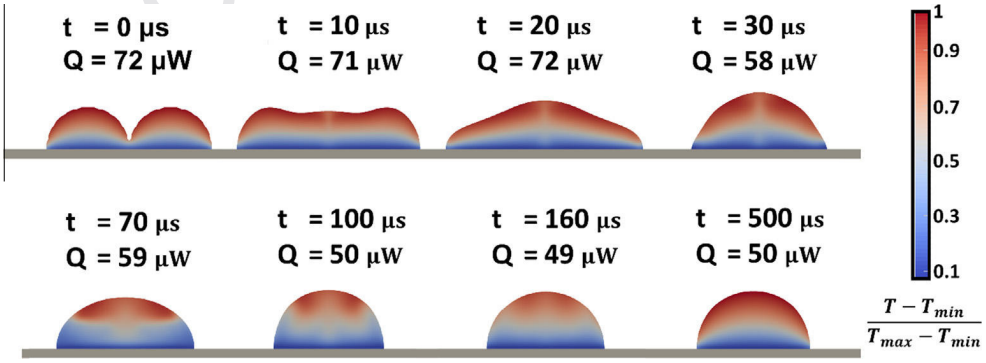

Fig. 1. Coalescing droplet mid-plane temperature profiles. Both parent droplet radii are 25 μm. The maximum velocity observed during coalescence is $U_{max} \sim 3\ ms^{-1}$.

$$\beta = \phi\beta_L + (1-\phi)\beta_V \quad \beta \in [\rho, \mu, k] \tag{2}$$

$$c_p = \frac{\phi c_{p,L}\rho_L + (1-\phi)c_{p,V}\rho_V}{\phi\rho_L + (1-\phi)\rho_V} \tag{3}$$

Here u_i is the velocity vector, $\dot{\phi}_{pc}$ is the volumetric phase fraction source due to condensation phase change, β represents the fluid property in a cell and the subscripts L and V represent the liquid phase and the vapor phase, respectively. ρ is the density, μ is the viscosity, k is the thermal conductivity, and c_p is the mass weighted specific heat capacity in a cell [34–36]. The fluid properties are assumed constant for the vapor and liquid phases.

The present simulations focus on the period between initiation of coalescence between two parent droplets and the recovery of a quasi-steady temperature profile in the child droplet. During this period, the increase in liquid volume in a droplet due to condensation is assumed to be small. Additionally, the momentum transfer from the condensing vapor to the droplets is relatively low. Therefore, the process can be modeled assuming incompressible flow (Eq. (4), $\dot{\phi}_{pc} = 0$) and by using the incompressible Navier-Stokes equation (Eq. (5)).

$$\frac{\partial u_i}{\partial x_i} = 0 \tag{4}$$

$$\frac{\partial(\rho u_i)}{\partial t} + \frac{\partial}{\partial x_j}(\rho u_i u_j) - \frac{\partial}{\partial x_j}\left[\mu\left(\frac{\partial u_i}{\partial x_j} + \frac{\partial u_j}{\partial x_i}\right)\right] = -\frac{\partial p}{\partial x_i} + \rho g_i + f_{s,i} \tag{5}$$

Here, g_i is the gravity vector and $f_{s,i}$ is the surface tension force (applied on a volumetric basis, described in Section 2.2).

The justification for the incompressible flow assumption is as follows. The characteristic velocities (V_c) due to droplet coalescence are much greater than the droplet growth rate ($\frac{dr}{dt}$). V_c is defined as the distance moved by the larger of the two droplets divided by the time it takes for the oscillations to die out. The droplet front velocity due to condensation phase change is $\frac{dr}{dt}$ (Eqs. (6) and (7)) [37]. Based on simulation results described later, for a water droplet with 1 μm diameter on a surface at 99.15 °C (T_{sat} = 100.15 °C) $V_c \sim 8.3$ ms^{-1}. The predicted droplet growth rate due to condensation is: $\frac{dr}{dt} \sim 8.4 \times 10^{-5}$ ms^{-1}. For similar conditions, a 1 mm droplet will have $V_c \approx 2.4 \times 10^{-3}$ ms^{-1} and $\frac{dr}{dt} = 6 \times 10^{-7}$ ms^{-1}.

$$\frac{dr}{dt} = \frac{\Delta T}{2\rho h_{LV}} \times \frac{1}{\frac{fr}{k} + \frac{1}{2h_i}} \tag{6}$$

$$h_i = \left(\frac{2\hat{\sigma}}{2-\hat{\sigma}}\right) * \left(\frac{h_{LV}^2}{T_V v_L}\right) * \left(\frac{M}{2\pi R T_V}\right)^{1/2} \tag{7}$$

Here, ΔT is the temperature difference between the cooled surface and the vapor, k is the thermal conductivity of the liquid, and $f = f(\mathrm{Bi}, \theta)$ is the coefficient for conduction resistance [31], h_i is the interfacial heat transfer coefficient, $\hat{\sigma}$ (0.03 [37]) is the accommodation constant, h_{LV} is the enthalpy of vaporization, T_V is the ambient temperature, M is the molecular mass of the working fluid, and R is the specific gas constant. The saturation temperature of the vapor at the ambient pressure (T_{sat}) is substituted for T_V in Eq. (7).

Similarly, the relative significance of the momentum imparted by steam vapor condensing into the interface can be assessed by comparing the vapor stagnation pressure $\left(\frac{1}{2}\rho_V\left[\frac{dr}{dt}(1+\rho_L/\rho_V)\right]^2\right)$ to the capillary pressure ($2\sigma/r$). For these cases, the vapor stagnation pressure (r = 1 μm, $\Delta p = 5 \times 10^{-3}$ Pa; r = 1 mm, $\Delta p = 3 \times 10^{-7}$ Pa) is negligible compared with the capillary pressure (r = 1 μm, $\Delta p = 1.2 \times 10^5$ Pa; r = 1 mm, $\Delta p = 1.2 \times 10^2$ Pa). Based on these arguments, the growth of the interface due to phase change and condensation of vapor into the interface do not affect the hydrodynamics of the problem, justifying the incompressible flow assumption.

Eq. (8) is the thermal energy equation, where k is the thermal conductivity and $\dot{q}_{pc}$ is the volumetric phase change heat source. Further details are provided in Section 2.3.

$$\frac{\partial(\rho C_p T)}{\partial t} + \frac{\partial}{\partial x_i}(\rho C_p u_i T) = \frac{\partial}{\partial x_i}\left[(C_p k)\frac{\partial T}{\partial x_i}\right] - \dot{q}_{pc} \tag{8}$$

2.2. Surface tension model

For the droplets size range of the present study Marangoni effects can be neglected [38,39]. Therefore, a constant surface tension value is assumed ($\sigma = 0.056$ N m^{-1}). Surface tension forces are calculated in each cell using the continuum surface tension force formulation (Eq. (9)) developed by Brackbill et al. [40]. Resulting momentum fluxes through cell faces are applied as an explicit source term in the pressure correction process.

$$f_{s,i} = \sigma\kappa\nabla\phi; \quad \kappa = -(\nabla\cdot\hat{n}); \quad \hat{n} = \frac{\nabla\phi}{|\nabla\phi|} \tag{9}$$

Here, σ is the surface tension between the liquid and the vapor phases, κ is the curvature at the interface, and $\hat{n}$ is the unit normal into the vapor phase. In the OpenFOAM VOF implementation, the interface is spread over a few cells; therefore, $\nabla\phi$ is effectively smoothed delta function which applies the force over the diffuse interface.

2.3. Phase change model

The phase change model is based on the approach of Rattner and Garimella [35]. The volumetric heat source $\dot{q}_{pc}$ is applied on interface cells (Eq. (8)).

$$\dot{q}_{pc} = \frac{h_i A \Delta T}{V_{cell}}; \quad A = |\nabla\phi|\cdot \mathrm{V}_{\mathrm{cell}} \tag{10}$$

Here, h_i is the interfacial heat transfer coefficient, A is an approximation of the area of the interface area contained in a cell, ΔT is the difference between the saturation temperature and the local temperature ($\Delta T = T_{sat} - T$), and V_{cell} is the volume of the cell. $\dot{q}_{pc}$ is solved implicitly as part of the energy equation (Eq. (8)). The foregoing heat transfer model has been validated by Adhikari et al. [31].

2.4. Dynamic contact angle model

A static contact angle model is insufficient to predict the process of coalescence because the three-phase contact line moves during the process. In general, the advancing contact angle θ_A, is greater than the static contact angle θ_0, which is greater than the receding contact angle θ_R (Fig. 2). To model the coalescence accurately, the dynamic contact angle model of Yokoi et al. (Eq. (11)) [41] is used:

$$\theta_D = \begin{cases} \min\left[\theta_0 + \left(\frac{\mathrm{Ca}}{\mathrm{k_a}}\right)^{\frac{1}{3}}, \theta_{\mathrm{ma}}\right] & \text{if } \mathrm{Ca} \geqslant 0 \\ \max\left[\theta_0 + \left(\frac{\mathrm{Ca}}{\mathrm{k_r}}\right)^{\frac{1}{3}}, \theta_{\mathrm{mr}}\right] & \text{if } \mathrm{Ca} < 0 \end{cases} \tag{11}$$

Here, θ_0 is the static contact angle, θ_D is the dynamic contact angle, $\mathrm{Ca} = \frac{\mu \mathrm{U_{cl}}}{\sigma}$ is the local capillary number, $\mathrm{U_{cl}}$ is the velocity of the moving contact line which is positive in the direction of the droplet outward normal vector ($\hat{n}$) on the condensing surface. $\mathrm{k_a}$ and $\mathrm{k_r}$ are liquid-surface pair dependent constants, θ_{ma} is the limit for advanc-

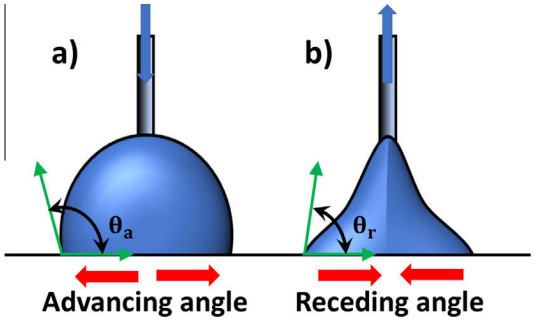

Fig. 2. Advancing and receding contact angles measured using volume changing technique (liquid injection or removal from the top of the droplet). (a) Increasing volume of the drop. (b) Decreasing volume of the drop.

ing contact angle, and θ_{mr} is the limit for receding contact angle. In the present study parameters for water-silicon (with hydrophobic silane grafted on it) are used, as listed by Yokoi et al. [41]. The surface parameters are as follows: $\theta_{ma} = 114^\circ$, $\theta_{mr} = 52^\circ, \theta = 90^\circ$; $k_a = 9 \times 10^{-9}$; and $k_r = 9 \times 10^{-8}$. The model, as implemented here, is validated with experimental data from [41] in Section 3.2.

2.5. Solution algorithm

The OpenFOAM® finite volume formulation is applied to discretize the governing equations, and the solution algorithm is summarized as a flow chart in Fig. 3. Expanded discussion of the phase change simulation approach is provided in the study by Nabil and Rattner [34].

3. Simulation studies

3.1. Studied domain and case setup

Coalescence of two droplets is symmetric along one center plane. Therefore, the domain only includes half of the droplets and their surrounding region. Fig. 4 shows the representative domain with labeled boundaries.

Here, $L = 6 \times r_1 + 2 \times Rt \times r_1$ and $W = H = 2 \times r_1 + Rt \times r_1$, r_1 is the radius of the smaller droplet, and Rt $\geqslant 1$ is the ratio of the two merging droplets. Table 1 shows the boundary conditions at the respective boundaries.

Here $\hat{n}_w$ is the unit normal from the wall pointing into the domain, $\hat{n}$ is the unit normal from the liquid phase to the vapor phase, and $\hat{p}$ is the unit normal to the patch. For wall $\hat{n}_w = \hat{p}$. The dynamic contact angle model is applied as a boundary condition for the phase fraction term ϕ. While the no-slip boundary condition is applied at the wall, in this finite volume formulation, the mean velocity in cells adjacent to the wall can be non-zero. This introduces enough numerical slip to eliminate the stress singularity at the three-phase contact line [42].

For the studied case of steam condensing at atmospheric pressure, >95% of the heat transfer occurs through droplets with $r < 100$ μm [4,6] – which is the radius of the largest droplet in this parametric study. Surface tension dominates gravity for such small droplets; therefore, the droplets can be initialized as truncated spheres [43].

For the studied range of droplet sizes (1 μm $< r <$ 100 μm) conduction is the primary mode of heat transfer [38]. Conduction is a diffusion process [44], and therefore, the thermal front takes a finite amount of time to propagate from the base of the droplet to the liquid vapor interface. An order of magnitude estimate of the conduction front propagation velocity is $\left(\frac{\alpha_l}{r}\right)$. This velocity is generally much greater than the droplet growth rate (Section 2.1). For example, for a water droplet with 1 μm diameter on a surface at 99.15 °C ($T_{sat} = 100.15$ °C) the conduction front velocity is $\frac{\alpha_l}{r} \sim 1.6 \times 10^{-1}$ ms^{-1}, whereas the droplet growth rate is

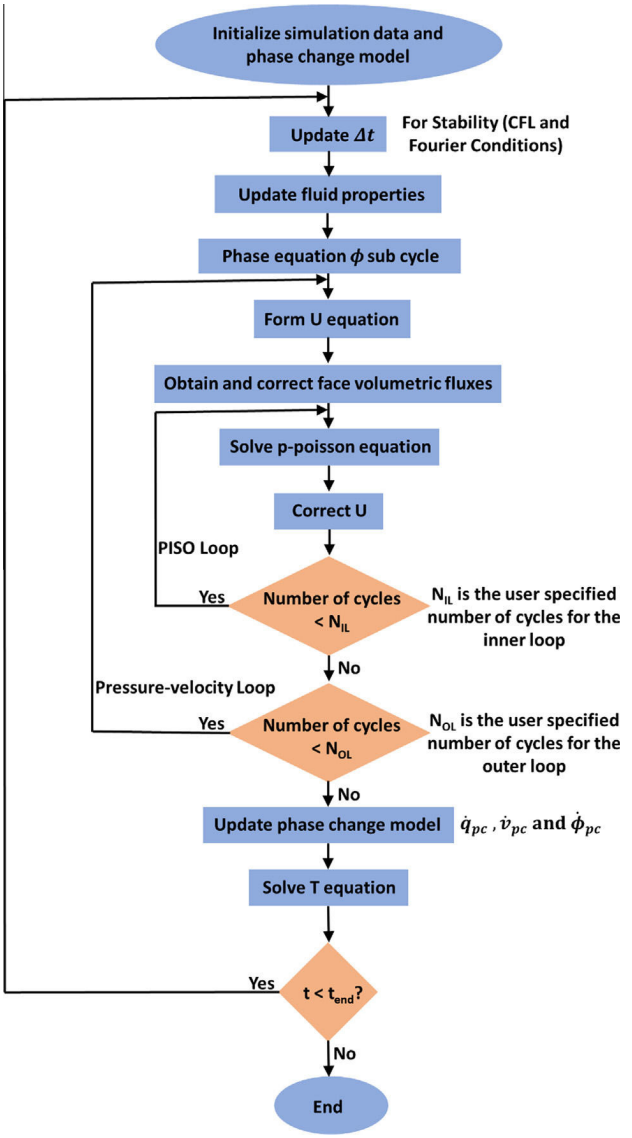

Fig. 3. Phase change volume-of-fluid solver algorithm flow chart.

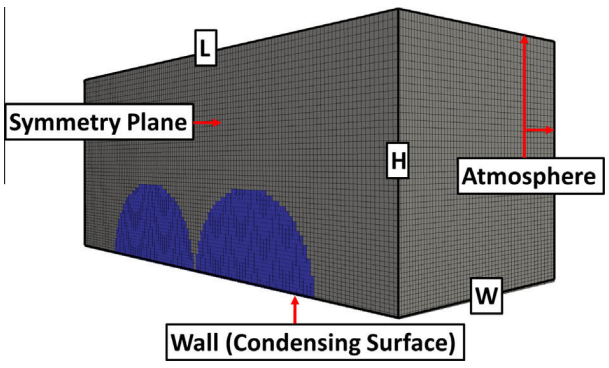

Fig. 4. Representative domain for the VOF coalescence study. The face showing the droplets is the symmetry plane; the bottom surface, which is not visible in the figure, is the condensing surface; and the remaining 4 faces are open atmosphere.

Table 1
Boundary conditions for the VOF simulation domain.

Boundary	Boundary condition
Symmetry	$\nabla T \cdot \hat{p} = 0$ $\nabla P \cdot \hat{p} = 0$ $U \cdot \hat{p} = 0; \nabla U \cdot \hat{p} = 0$ $\nabla \phi \cdot \hat{p} = 0$
Atmosphere	$\nabla T \cdot \hat{p} = 0$ $P = P_{atm}$ $\nabla U \cdot \hat{p} = 0$ $\nabla \phi \cdot \hat{p} = 0$
Wall (condensing surface)	$T = (T_{sat} - 1\ \mathrm{K})$ $\nabla P \cdot \hat{p} = 0$ $U = 0$ $\hat{n} \cdot \hat{n}_w = \cos(\theta_D)$

$\frac{dr}{dt} \sim 8.4 \times 10^{-5}$ ms^{-1}. Based on the arguments, a quasi-steady state internal temperature distribution can be assumed in droplets just before coalescence begins. Therefore, the droplets are initialized with a steady-state temperature distribution (Fig. 5), obtained by solving the steady-state energy equation (Eq. (12)).

$$\frac{\partial}{\partial x_i \partial x_i}(kT) = \dot{q}_{pc} \tag{12}$$

3.2. Grid resolution, sensitivity study and dynamic contact angle validation

The mesh resolution must be sufficient to resolve heat transfer and hydrodynamic effects. Fig. 6 shows the representative droplet isosurfaces with VOF meshing, for the parametric study. The mesh is made of cube cells, and extends similarly in the third dimension.

Grid resolution in the domain is defined using $n_r = (number\ of\ cells)/r_1$. Conduction grid independence studies are carried out for the largest and the smallest radii droplets ($r_1 = 1$ μm and $r_1 = 25$ μm). n_r is varied from 5 to 21, and the heat transfer rate (Q) through the base of the droplets is evaluated. For each mesh in the grid sensitivity study, n_r is increased by a factor of 1.6 (total number of cells increases by 4×). Q is plotted against n_r. In both the cases, it is observed that Q becomes asymptotic (Richardson extrapolated values of Q are given in the supplemental data available publicly [45]) when $n_r \in [13, 21]$ (Fig. 7). The uncertainties for Q in both the cases are less than 0.4%. Therefore, $n_r = 15$ can be assumed the minimum resolution for heat transfer in the parametric study (Fig. 6c). As an example, for a droplet of radius 1 μm and $n_r = 15$, average length of a mesh element $\Delta = 6.67 \times 10^{-8}$ m.

To study hydrodynamic grid independence, and also to verify the selected dynamic contact angle model, an axisymmetric droplet impact simulation is performed for the case of [41,42]. In the simulation a 2.28 mm diameter spherical water droplet impacts a surface with a velocity of 1 ms^{-1}. The surface properties are given in Section 2.4, and the fluid properties are as follows:

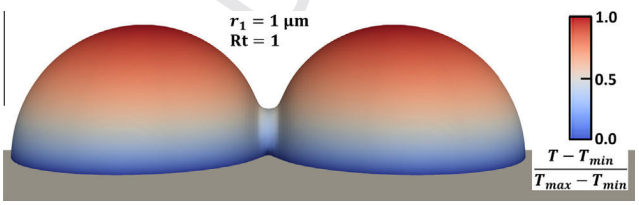

Fig. 5. Steady state temperature distribution on the droplet surfaces before merging.

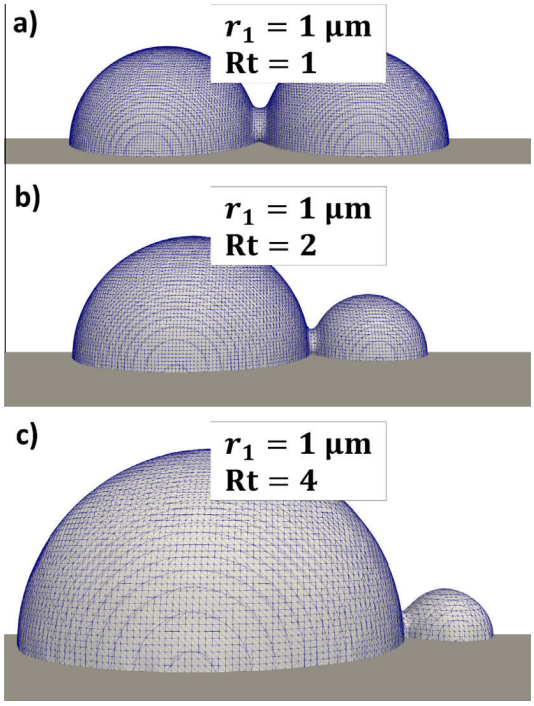

Fig. 6. Representative droplet isosurfaces, indicating VOF mesh resolutions for the droplets from the parametric study. (a) For smaller droplet radius $r_1 = 1$ μm and radius ratio Rt = 1. (b) For $r_1 = 1$ μm and Rt = 2. (c) For $r_1 = 1$ μm and Rt = 4.

dynamic viscosity liquid $\mu_l = 1 \times 10^{-3}$ kg m^{-1} s^{-1} ; dynamic viscosity air $\mu_g = 1.82 \times 10^{-5}$ kg m^{-1} s^{-1} ; $\sigma = 0.072$ N m^{-1}. n_r for the axisymmetric study is varied from 19 to 55. Fig. 8 presents the variation of average diameter D (square root of the base area) of the impacting droplet as a function of time for different grid resolutions. Experimental data [41] is also presented. It is observed that the average absolute deviation (AAD) for D from $n_r = 38$ to $n_r = 55$ is less than 3%. Since, in the parametric study, the droplets merge and oscillate together as a larger droplet before settling, $n_r = 40$ is selected as the minimum resolution for the parametric study (Fig. 6a), which is a stricter requirement than imposed by the heat transfer process alone.

4. Validation of results

Response time and spatial resolution requirements make it difficult to study the process of droplet coalescence experimentally. For example, in the present study: 1 μm $< r <$ 100 μm, and the times of coalescence are only 0.5 μs $< 4 \times |\tau| <$ 1.2 ms. During the startup of dropwise condensation on a surface, droplets could be even smaller. Owing to these challenges, there are no experimental or computational studies available to validate the time-varying heat-transfer during coalescence. However, the steady state heat transfer results from this simulation (just before and long after coalescence) can be compared with published steady-state conduction heat transfer simulation data from Sadhal and Martin [30] to validate the heat transfer formulation used in the study.

Steady condensation heat transfer rates for water droplets of r = 1–100 μm radii (the range of sizes studied here) from this simulation study are compared with results from [30]. The average absolute deviation (AD) from that study is less than 3%. The comparison is given in Fig. 9, where the total heat transferred through the base of the droplet (Q) is plotted against the Biot number

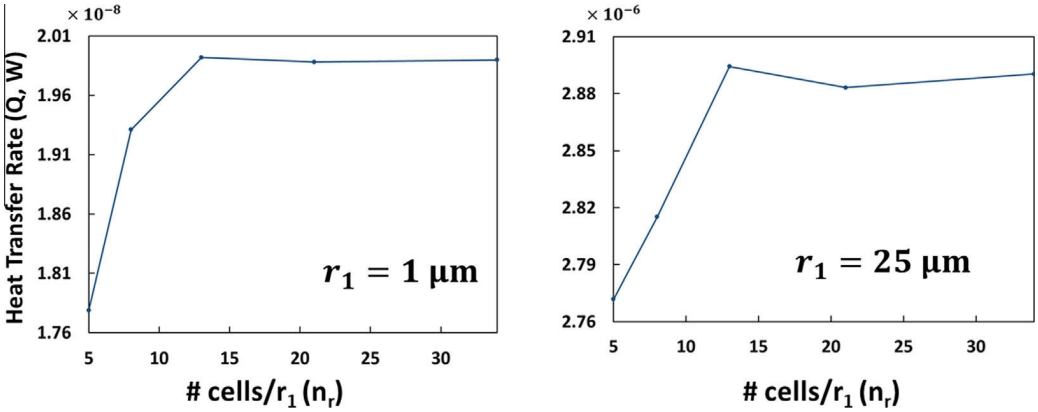

Fig. 7. Heat transfer grid independence study (Q vs n_r where $n_r = \#\ cells/r_1$) for $r_1 = 1$ μm and $r_1 = 25$ μm.

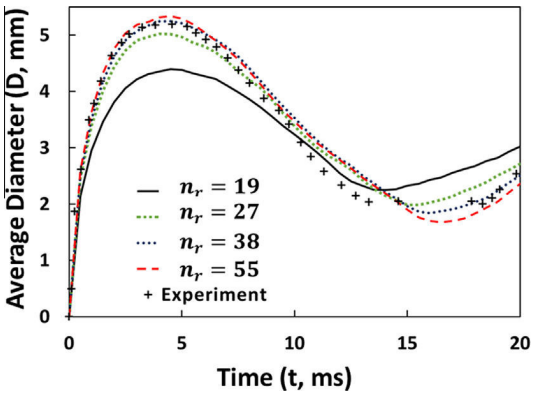

Fig. 8. Colliding droplet contact patch diameter on surface (D) vs. time (t) for different grid resolutions and experimental data [41].

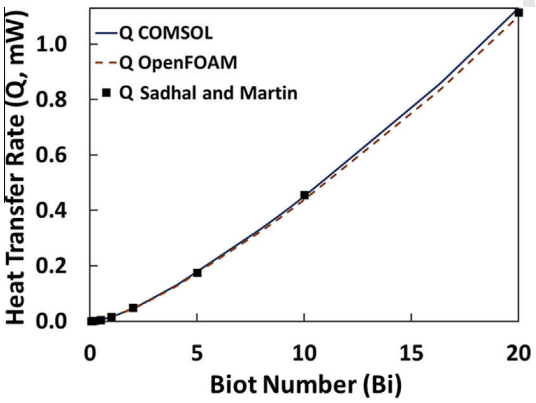

Fig. 9. Comparison of the simulation data (heat transfer rate (Q) vs. Biot number (Bi)) with that of Sadhal and Martin [30], and conduction-only finite element COMSOL simulations.

($Bi = \frac{h_i r}{k}$) of the droplet. Here h_i is the interfacial heat transfer coefficient, r is the radius, and k is the thermal conductivity of the droplet. Bi corresponds directly to r in the simulation as h_i and k are fixed.

A finite element conduction heat transfer analysis is also performed for droplets of r = 1–100 μm to further validate the simulation heat transfer formulation. For the studied range of droplet sizes Marangoni circulation and other convection effects can be neglected [38]. Therefore, the finite element analysis reduces to a simple conduction problem in truncated spheres (Section 3.1). The droplets are evaluated with 2-D axisymmetric domains (Fig. 10). A fixed temperature boundary condition is applied on the base of the axisymmetric droplet domain (1 K below the saturation temperature), representing the cooled condenser surface temperature. A convection boundary condition is applied to the liquid-vapor interface to account for interfacial resistance h_i. The conduction studies were performed in COMSOL Multiphysics® (v. 5.2 [46]).

Grid sensitivity study was performed for each finite element case where three meshes were utilized to extrapolate the converged value of total heat transfer Q through the base of any droplet. The method is given by Celik et al. [47], and is briefly described here.

Meshes (Fig. 10) with average element dimensions: $\Delta_3 = 1.97 \times 10^{-9}$ μm – 1.99×10^{-5} μm, $\Delta_2 = 5.84 \times 10^{-10}$ μm–5.90×10^{-6} μm and $\Delta_1 = 1.48 \times 10^{-10}$ μm – 1.50×10^{-6} μm are employed. Subscript 3 refers to the coarsest mesh and subscript 1 refers to the finest mesh. The steps are as follows:

$$\varepsilon_{32} = Q_3 - Q_2;\ \varepsilon_{21} = Q_2 - Q_1;\ s = sgn\left(\frac{\varepsilon_{32}}{\varepsilon_{21}}\right) \tag{13}$$

$$R_{32} = \frac{\Delta_3}{\Delta_2};\ R_{21} = \frac{\Delta_2}{\Delta_1} \tag{14}$$

$$q(p) = \ln\left(\frac{R_{21}^p - s}{R_{32}^p - s}\right);\ p(q) = \frac{\left|\ln\left(\left|\frac{\varepsilon_{32}}{\varepsilon_{21}}\right|\right) + q\right|}{\ln(R_{21})} \tag{15}$$

$$Q_{ext} = (R_{21}^p Q_1 - Q_2)/(R_{21}^p - 1) \tag{16}$$

$$e_a^{21} = \left|\frac{Q_1 - Q_2}{Q_1}\right|;\ \mathrm{GCI} = \frac{1.25 e_a^{21}}{R_{21}^p - 1} \tag{17}$$

$$unc = \mathrm{Q_{ext}} \times \mathrm{GCI} \tag{18}$$

The ε values are the changes in Q between meshes. R values are the mesh refinement ratios. p is the empirical convergence rate, defined implicitly in terms of parameter q. Q_{ext} is the extrapolated value of Q for $\Delta \to 0$ (infinitely fine mesh). e_a^{21} is the relative error between the two finest meshes. GCI is the grid convergence index, a relative uncertainty estimate for Q_{ext}. The absolute uncertainty unc in Q_{ext} is determined from Eq. (18).

All studied cases were found to be monotonically converging ($s = 1$) and therefore the grid convergence index (GCI) uncertainty estimate for Q_{ext} was reported (<0.2% uncertainty in all cases). Fig. 9 shows the comparison with simulation results.

Please cite this article in press as: S. Adhikari, A.S. Rattner, Heat transfer during condensing droplet coalescence, Int. J. Heat Mass Transfer (2018), https://doi.org/10.1016/j.ijheatmasstransfer.2018.07.005

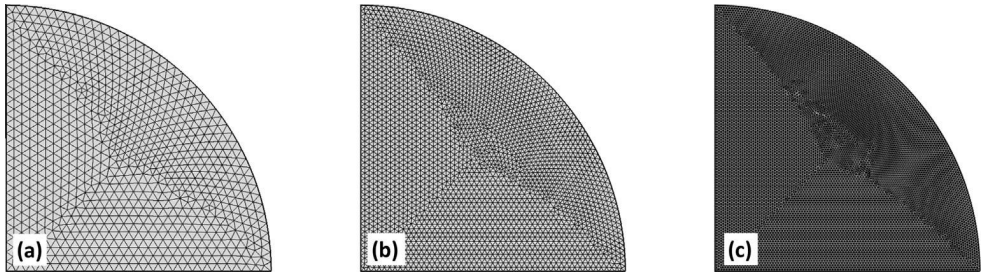

Fig. 10. Representative mesh sizes: (a) coarse $\Delta_3 = 1.97 \times 10^{-9}$ μm – 1.99×10^{-5} μm; (b) fine $\Delta_2 = 5.84 \times 10^{-10}$ μm – 5.90×10^{-6} μm; (c) finest $\Delta_1 = 1.48 \times 10^{-10}$ μm – 1.50×10^{-6} μm.

The hydrodynamics (Fig. 8) and steady-state heat transfer rates (Fig. 7) are both separately validated. This supports the validity of the simulation approach for predicting transient heat-transfer in coalescing droplets.

4.1. Results and discussion

Fig. 1 shows a representative time series evolution of surface temperature profiles as two parent droplets (r_1 = 25 μm; Rt = 1) merge together to form a new child droplet. Heat transfer through the base of the merging droplets is presented. Initially, the droplets have quasi-steady temperature profiles, which are disturbed at the start of coalescence. When the two droplets come in contact, a liquid bridge forms (Fig. 1, 0 μs). The bridge initially has concave curvature, resulting in a local low-pressure zone due to surface tension forces. Liquid flows from the outer high pressure regions in the parent droplets toward the low pressure region in the bridge [48] (0–20 μs). Due to contact angle hysteresis, the outer portion of the three-phase contact line does not begin to move until well after the start of coalescence (~25 μs). At this point, the child droplet begins oscillating on the condensing surface (30–200 μs). The oscillations gradually reduce in intensity due to viscous dissipation within the droplet. The temperature profile within the droplet also decays toward a quasi-steady profile (Fig. 1, 500 μs). For these simulations of water condensing at atmospheric pressure, the oscillation period and the heat transfer decay period are found to be approximately equal.

A decaying exponential function, with time constant τ, can be used to represent the time varying average heat flux through the child droplet. A parametric study is performed in Section 5.3 to characterize heat flux trends in coalescing droplets over a range of sizes (r_1) and radius ratios ($R_t = r_2/r_1$). Table 2 provides the simulation test matrix and along with the values of τ obtained from the simulations. The working fluid is saturated water at atmospheric pressure.

Table 2
Simulation test matrix for the parametric study of coalescing droplets, with varying smaller radius (r_1) and the ratio between the radii of the merging droplets (Rt). Time constant τ is obtained from the simulation results.

Droplet Radii [μm]		Ratio ($Rt = r_2/r_1$)	Time constant (τ) [μs]
r_1	r_2		
1	1	1	0.129
1	2	2	0.357
1	4	4	0.650
6.25	6.25	1	5.80
6.25	12.5	2	16.1
6.25	25	4	28.9
25	25	1	65.9
25	50	2	170
25	100	4	287

The following sections characterize the process of coalescence and propose trends for the stabilization time of coalescing water droplets at atmospheric pressure for the studied range of droplet sizes and surface parameters. The impact of coalescence on condensation heat transfer is assessed considering direct heat transfer through a child droplet (direct mechanism), and repeated clearing of the surrounding surface as the droplet oscillates (indirect mechanism).

4.2. Characterizing coalescence

In dropwise condensation, latent heat from the condensation process transfers through the liquid-vapor interface (interfacial resistance R''_{int}) and then conducts through the droplet to the cooled wall (R_{cond}). Some studies have argued that the overall single droplet heat transfer rate depends on the three-phase contact line length [49–51], as most of the heat is transferred through the perimeter of the droplet, near the condenser surface (Fig. 5). This result applies for droplets with high Bi (Biot number $Bi = \frac{h_i r}{k}$), for which conduction resistance is much greater than the interfacial resistance. However, for cases where the conduction resistance is comparable with the interfacial resistance (low *Bi*), significant conduction occurs through the entire base of the droplet, and not just the contact-line region. Fig. 11 shows the dependence of heat transfer on the droplet radius. The working fluid for the figure is saturated water at atmospheric pressure. The calculations were based on the heat transfer model of Adhikari et al. [31].

The form of the curve in Fig. 11, for the range $r \in [3 \times 10^{-10}, 3 \times 10^{-4}]$ m ($Q \in [1 \times 10^{-12}, 1]$ W), is approximately

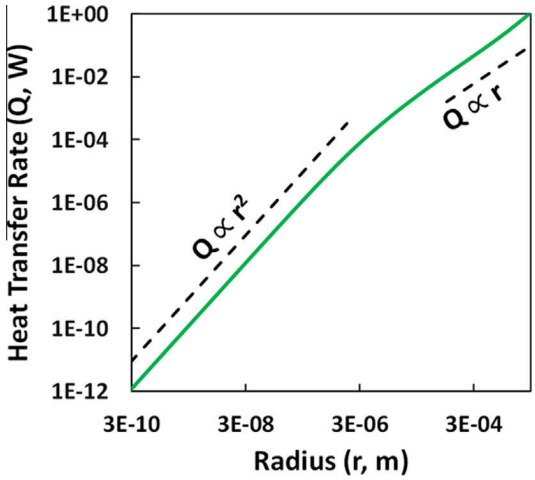

Fig. 11. Total heat transfer rate (Q) vs. droplet radius (r) for water condensation at atmospheric pressure. The dashed lines indicate the rate of variation of heat transfer with droplet radius for different size droplets.

quadratic (*i.e.*, $Q \propto r^2$). This suggests that for smaller droplets, heat transfer is proportional to base area.

Fig. 12 compares the time variation of the heat transferred through two equal size coalescing droplets with $r_1 = r_2 = 6.25$ μm ($Bi \approx 0.3$) with the time variation of the base area of the merging droplets and the perimeter length of the contact line. It is clear from the comparison that heat transfer rate is proportional to base area during the coalescence of water droplets of this size range.

A slight increase in the heat transfer is observed shortly after the beginning of coalescence. This occurs because the total base area briefly increases while the liquid bridge grows, but the outer contact line sections are still pinned due to hysteresis. Once the hysteresis effect is overcome, the droplet base area and heat transfer sharply decrease, and then oscillate in-sync.

A Finite Fourier Transform (FFT) can be applied to transient heat transfer traces to extract the principal frequencies in the oscillating

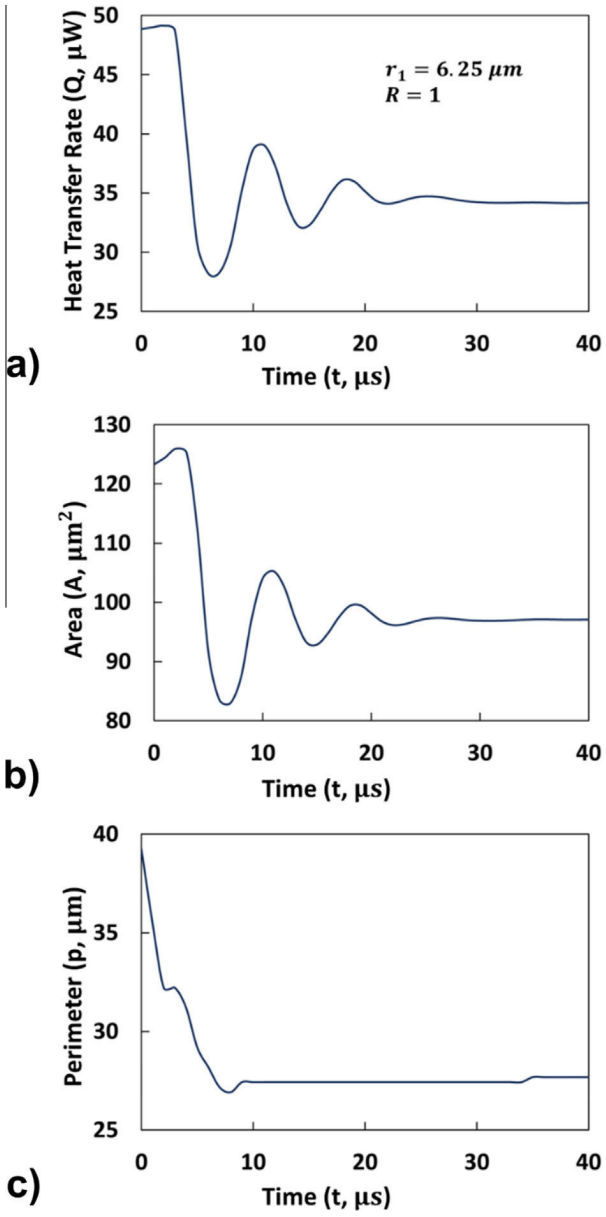

Fig. 12. Comparison of (a) condensing droplet heat transfer rate vs. time, (b) base area vs. time, and (c) contact line (perimeter) length vs. time for two merging drops of radii 6.25 μm ($Bi \approx 0.3$).

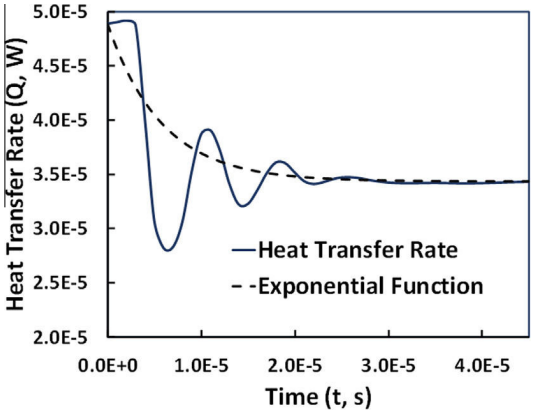

Fig. 13. Decaying exponential function superimposed over Q vs Time plot of two equal merging drops of radii 6.25 μm each.

coalescence process. As an example, the principal frequency of the time varying heat transfer through droplets ($R_1 = R_2 = 1$ μm) is 1×10^5 Hz. The average heat transfer trend can be approximated with a decaying exponential function (Fig. 13), neglecting this oscillatory component.

Fig. 13 presents the best-fit decaying exponential function and the oscillatory time-varying heat transfer through the base of two merging droplets ($r_1 = r_2 = 6.25$ μm; time constant $\tau = 5.8 \times 10^{-6}$ *s*). This heat transfer decay rate could be incorporated into Lagrangian-type models of the overall dropwise condensation process [8] to more accurately account for transient heat transfer after coalescence events, rather than assuming a step change from the quasi-steady heat transfer rate of the two parent droplets to that of the single child droplet.

4.3. Effect of coalescence on heat transfer

If a dropwise condensation model assumes instantaneous merging and recovery of quasi-steady heat transfer for a pair of droplets, it will under-predict the total heat transfer. The resulting heat transfer deficit is due to a step-change assumption is:

$$\mathrm{Def} = \left(\frac{\int_0^{t_{\mathrm{coalesce}}} a e^{-\frac{t}{\tau}} dt}{\int_0^{t_{\mathrm{coalesce}}} a e^{-\frac{t}{\tau}} dt + c t_{\mathrm{coalesce}}} \right) \times 100\%. \quad (19)$$

Here, a is the difference in the steady state heat transfer between that of the two parent droplets and the child droplet. c is the steady state heat transfer for the child droplet. The decaying heat transfer is integrated from time $t = 0$ to $t = t_{\mathrm{coalesce}}$ – the time for the child droplet to settle to a steady heat transfer rate.

This heat transfer deficit effect is illustrated for two representative cases: (1) $r_1 = 1$ μm, $\mathrm{Rt} = 1$ and (2) $r_1 = 25$ μm, $\mathrm{Rt} = 4$. For cases 1 and 2, $\mathrm{Def}_1 \sim 8\%$ and $\mathrm{Def}_2 \sim 5\%$. This deficit could become significant if many droplets are coalescing on a surface.

Assuming instantaneous droplet coalescence thus causes a modest under-prediction of heat transfer by neglecting the thermal stabilization time of the child droplet. This could be termed as the *direct mechanism* of heat transfer enhancement due to coalescence. However, merging droplet hydrodynamics can cause a second *indirect* heat transfer enhancement mechanism. As merging droplets oscillate before stabilizing, they repeatedly clear small droplets from surrounding surface area, and initiate periodic renucleation in this swept area. Local condensation heat flux can be very high right after droplets are cleared from a region. Therefore, this indirect heat transfer enhance mechanism may be even more significant than the direct mechanism.

Please cite this article in press as: S. Adhikari, A.S. Rattner, Heat transfer during condensing droplet coalescence, Int. J. Heat Mass Transfer (2018), https://doi.org/10.1016/j.ijheatmasstransfer.2018.07.005

Glicksman and Hunt [28] performed a numerical study of the dropwise condensation process from initialization on a dry surface, yielding transient heat transfer trends. Data from their study is adopted here in this paper to estimate the *indirect* heat transfer enhancement mechanism (curve fit to their data in Eq. (20)). Their data are for saturated water at atmospheric pressure ($T_{sat} = 100\,^{\circ}C$) with a condensing surface 0.28 °C below the T_{sat}. Nucleation site density was assumed to be 10^9 cm^{-2}.

$$q''_{SGS}(t) = (8.379 \times 10^5\ \mathrm{W\ m^{-2}})\left(\frac{t}{1\mathrm{s}}\right)^{-0.2356} \quad (20)$$

Here, t represents the time since the condensing surface was initially dry. The transient heat flux trend from [28] ($q''_{SGS}(t)$) is applied as a sub-grid scale model on portions of the wall not covered by grid scale droplets in the VOF simulation. This heat flux represents the heat transfer from condensing small droplets around the studied grid-scale droplets. Here, $q''_{SGS}(t)$ is evaluated for every cell face on the wall boundary. A local time (t) is evaluated for each face as the time since it was last covered by a *grid-scale* droplet. q''_{SGS} is set to zero when a wall face is covered by a *grid-scale* droplet. Thus, this model captures the effect of merging droplets periodically sweeping the surface around them and re-initializing nucleation in the swept area.

This sub-grid scale model is evaluated for two cases with $r_1 = 25$ μm; Rt = 1. In the first case, two droplets coalesce and oscillate, as described in Section 5.1. The sub-grid scale heat flux value on the wall faces is initialized to 0. A second case represents the results of assuming instantaneous coalescence. Here, a single stationary droplet (same total liquid volume as in case 1) is placed in the center of the domain with a quasi-steady temperature distribution. The sub-grid scale heat flux value on the wall is initialized to 0, except for the area under the two parent droplets, which are set to t = 0 s. The heat flux in these cells evolves over time according to Eq. (20). The difference in heat transfer between the two cases (oscillating interface tracked droplet coalescence case and the static case) serves as an estimate of the heat transfer underprediction by assuming instantaneous coalescence. This resulting indirect heat transfer deficit is:

$$\mathrm{Def}_{\mathrm{indirect}} = \left(\frac{\int_0^{t_{coalesce}} q''_{SGS\_Dynamic}\,dt - \int_0^{t_{coalesce}} q''_{SGS\_Static}\,dt}{\int_0^{t_{coalesce}} q''_{SGS\_Static}\,dt}\right) \times 100\% \quad (21)$$

Fig. 14 shows the different trends of sub-grid scale heat transfer between the dynamic case and the static case. Fig. 14a shows the dynamic case in which the oscillating child droplet repeatedly clears sections of the wall, reinitializing nucleation and high heat

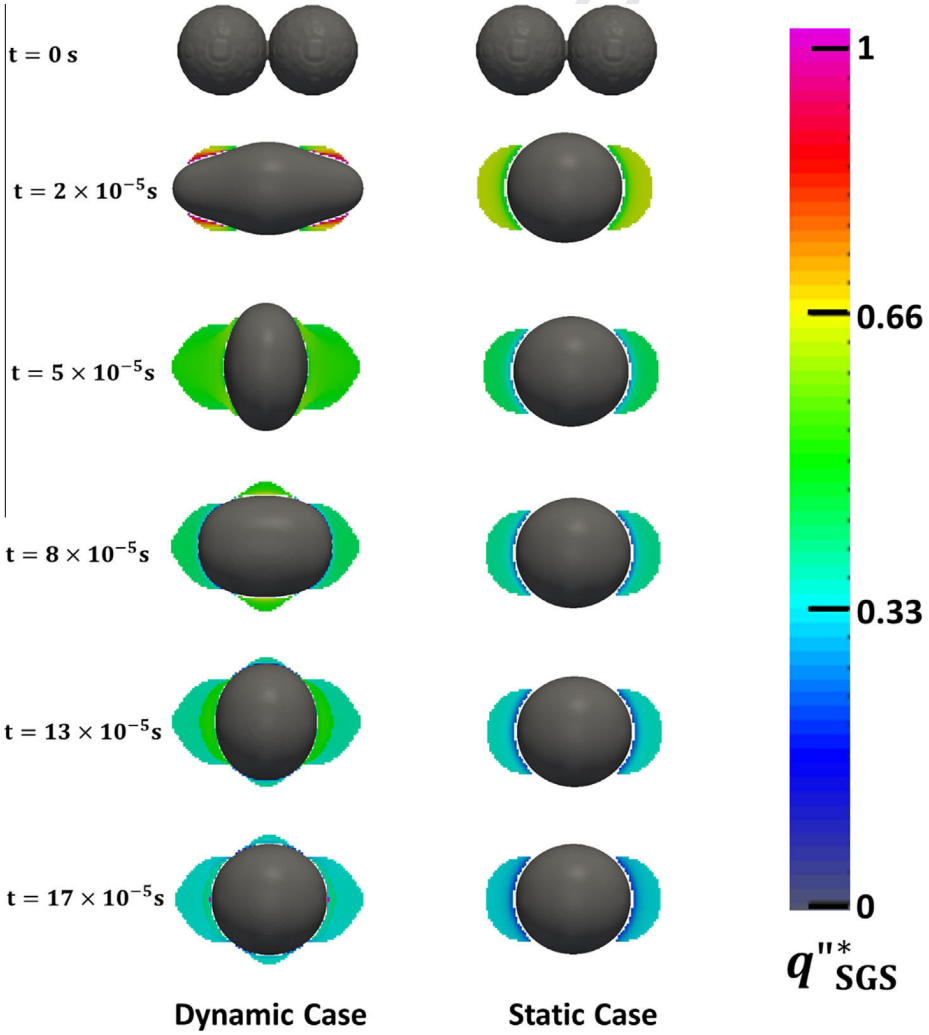

Fig. 14. Differences between subgrid-scale heat transfer due to microscale condensing droplets around two coalescing r = 25 μm droplets: (a) the dynamic coalescence case; and (b) the static coalescence case. Top-down view snapshots of the droplet shapes, represented in black, are presented. The colored area underneath the droplets shows the evolution of *sub-grid scale* heat flux due to small condensing droplets around the primary coalescing droplets $\left(q''^{*}_{SGS}(t) = \frac{q''_{SGS} - \min(q''_{SGS}(t))}{\max(q''_{SGS}(t)) - \min(q''_{SGS}(t))}\right)$.

Please cite this article in press as: S. Adhikari, A.S. Rattner, Heat transfer during condensing droplet coalescence, Int. J. Heat Mass Transfer (2018), https://doi.org/10.1016/j.ijheatmasstransfer.2018.07.005

fluxes. For the static case (Fig. 14b), however, $q''_{SGS}(t)$ is only non-zero on that exposed area that was previously under the parent droplets.

The heat transfer trends for the two cases are presented in Fig. 15. After 350 μs, when the oscillations in the droplet have almost died out, the heat transfer deficit approaches $\mathrm{Def}_{\mathrm{indirect}} \sim 11\%$, which is greater than the direct deficit. Unlike the direct deficit, the magnitude of this indirect deficit is expected to increase for larger oscillating droplets.

4.4. Simulation data and proposed correlation for droplet coalescence time constant

Simulation data for $\tau(r_1, \mathrm{Rt})$ from the parametric study cases listed in Table 2 were used to form a correlation (Eq. (22)) for τ for coalescence of condensing water droplets at atmospheric pressure on the studied hydrophobic silane surface. τ and r_1 were non-dimensionalized ($\tau^* = \tau\rho\sigma^2/\mu^3$; $r_1^* = \sigma\rho r_1/\mu_2$) using the simulation parameters ρ, σ and μ (for water at 1 atm), and a correlation was formed for $\tau^*(r_1^*, \mathrm{Rt})$. Table 3 lists the constants given in Eq. (22). Correlation τ^* vs. r_1^* curves for varying Rt are compared with simulation data (markers) in Fig. 16.

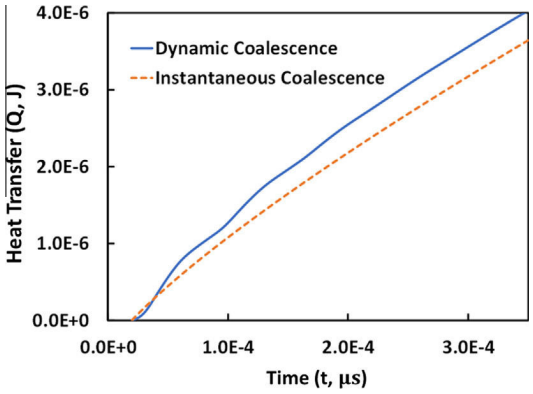

Fig. 15. Cumulative heat transfer for an interface tracked dynamic coalescence case and a static case. Initially, for both cases, both droplets have radius $r = 25$ μm.

Table 3
Constants for the droplet coalescence time constant correlation (Eq. (22)).

Constant	Value
a	0.063
b	1.927
c	1.144

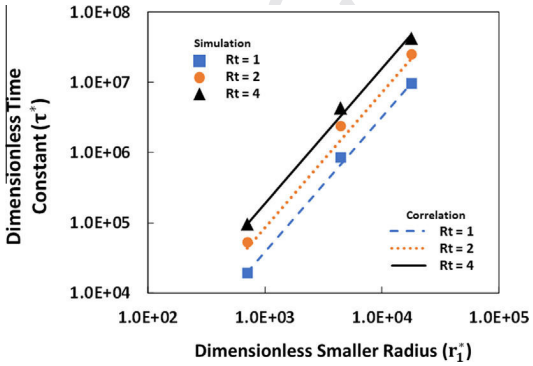

Fig. 16. Dimensionless time constant (τ^*) vs. dimensionless smaller droplet radius (r_1^*) and droplet radius ratio Rt. The curves are generated using the correlation given in Eq. (22) and the simulation data is represented by the markers.

Table 4
τ for representative test cases obtained from best-fit exponential curves to the experimental data and the proposed correlation (Eq. (22)).

r_1 [μm]	Rt	τ Simulation [μs]	τ correlation [μs]	AD (%)
3	1	1.36	1.11	18
12.5	2	53.61	38.34	28

$$\tau^* = a \times r_1^{*b} \times \mathrm{Rt}^c \quad (22)$$

The absolute average deviation (AAD) between the correlation and the data is 14%, and the maximum error is 37%. This represents reasonable agreement considering the three order of magnitude range of τ^* in the study space.

Two additional test cases: (1) $r_1 = 3$ μm, Rt = 1, and (2) $r_1 = 12.5$μm, Rt = 2, were simulated to assess the correlation given in Eq. (22). The comparison is provided in Table 4. The relative deviation for both cases is less than 30%.

5. Conclusions

In this study, a VOF formulation was proposed and validated for interface dynamics predictions (droplet impact) and steady state droplet condensation heat transfer. This method was then applied to simulate the process of water droplet coalescence during dropwise condensation for 9 cases over a range of radii ($1\ \mu\mathrm{m} \leqslant r \leqslant 100\ \mu\mathrm{m}$) and radius ratios ($1 \leqslant \mathrm{Rt} \leqslant 4$). Results were used to determine the time constant for droplet stabilization and transient heat transfer trends after dropwise condensation. The working fluid in this study was saturated water at atmospheric pressure. The surface properties (hydrophobic silane) were adopted from the study of Yokoi et al. [41].

Two mechanisms (Section 5.2) were identified for heat transfer enhancement due to droplet coalescence. The *direct* mechanism is due to the gradual decay of heat transfer from the quasi-steady rate for the two parent droplets to that of the larger child droplet. Instantaneous droplet coalescence models neglect this thermal stabilization time for the child droplet, and therefore under-predict droplet heat transfer by 5–10% during the period of coalescence. The *indirect* mechanism is due to the oscillating child droplet repeatedly clearing small droplets from the surrounding wall area, reinitializing nucleation in those areas. For two coalescing droplets of equal radii ($r_1 = 25$ μm), heat transfer enhancement due to the indirect mechanism is ~11%. This indirect effect may be even greater in larger droplets that oscillate over larger areas and have more momentum (longer oscillation periods).

A correlation for $\tau(r_1, \mathrm{Rt})$ was presented for the studied range of droplet sizes, fluid properties, and surface conditions. Two test cases ($r_1 = 3$ μm, Rt = 1 and $r_1 = 12.5$ μm, Rt = 2) were simulated to test the accuracy of the correlation, and satisfactory agreement was found.

Prior theoretical and numerical studies of dropwise condensation have generally assumed droplet coalescence to be instantaneous, and that child droplets immediately recover quasi-steady internal temperature profiles (no history effect) [28,52]. The present study used a direct interface tracking simulation technique to characterize the process of droplet coalescence and post-coalescence heat transfer trends. Findings suggest that the assumption of instantaneous coalescence underestimates the total heat transfer (direct underprediction + indirect underprediction due to the oscillating child droplet sweeping the area underneath) in the time shortly after droplet coalescence by 15–20%. Results from this study provide an improved closure model for droplet

Please cite this article in press as: S. Adhikari, A.S. Rattner, Heat transfer during condensing droplet coalescence, Int. J. Heat Mass Transfer (2018), https://doi.org/10.1016/j.ijheatmasstransfer.2018.07.005

coalescence that can be incorporated into Lagrangian dropwise condensation models to improve overall heat transfer predictions. Such improved dropwise condensation models may provide insights into the effects of coalescence and oscillating droplet dynamics on overall surface heat transfer.

Future investigations are warranted to expand results for coalescing droplet dynamics and heat transfer to a broader range of fluids and surfaces. Investigation of more complex coalescence dynamics is also needed, such as a cascade of coalescence events initiated by merging of a single droplet pair. If these complex droplet coalescence processes are better understood, it may be possible to enhance dropwise condensation heat transfer through surface engineering. For example, if contact angle hysteresis can be reduced, the oscillation time and spatial span of coalescing droplets may increase, amplifying the two heat transfer enhancement mechanisms identified in this study.

Conflict of interest

The authors declare that there are no conflicts of interest.

Acknowledgements

We wish to acknowledge generous support for this research by the US National Science Foundation under grant: CBET-1652578.

Appendix A. Supplementary material

Supplementary data associated with this article can be found, in the online version, at https://doi.org/10.1016/j.ijheatmasstransfer.2018.07.005.

References

[1] J.M. Beér, High efficiency electric power generation: the environmental role, Prog. Energy Combust. Sci. 33 (2) (2007) 107–134.
[2] J.R. Lara, G. Noyes, M.T. Holtzapple, An investigation of high operating temperatures in mechanical vapor-compression desalination, Desalination 227 (1) (2008) 217–232.
[3] T.B. Peters et al., Design of an integrated loop heat pipe air-cooled heat exchanger for high performance electronics, IEEE Trans. Components, Packag. Manuf. Technol. 2 (10) (2012) 1637–1648.
[4] E.J. Le Fevre, J.W. Rose, An experimental study of heat transfer by dropwise condensation, Int. J. Heat Mass Transf. 8 (8) (1965) 1117–1133.
[5] F.L. Shea, N.W. Krase, Drop-wise and film condensation of steam, Trans. AIChE 36 (1940) 463–490.
[6] C. Graham, P. Griffith, Drop size distributions and heat transfer in dropwise condensation, Int. J. Heat Mass Transf. 16 (2) (1973) 337–346.
[7] J.W. Rose, Dropwise condensation theory, Int. J. Heat Mass Transf. 24 (2) (1981) 191–194.
[8] J.W. Rose, "Dropwise condensation theory and experiment: a review, Proc. Inst. Mech. Eng. Part A J. Power Energy 216 (2) (2002) 115–128.
[9] D. Beysens, C.M. Knobler, Growth of breath figures, Phys. Rev. Lett. 57 (12) (1986) 1433–1436.
[10] R.N. Leach, F. Stevens, S.C. Langford, J.T. Dickinson, Dropwise condensation: experiments and simulations of nucleation and growth of water drops in a cooling system, Langmuir 22 (2006) 8864–8872.
[11] F. Chu, X. Wu, Y. Zhu, Z. Yuan, Relationship between condensed droplet coalescence and surface wettability, Int. J. Heat Mass Transf. 111 (2017) 836–841.
[12] J.E. Sprittles, Y.D. Shikhmurzaev, Coalescence of liquid drops: different models versus experiment, Phys. Fluids 24 (12) (2012).
[13] J.E. Sprittles, Y.D. Shikhmurzaev, Finite element framework for describing dynamic wetting phenomena, Int. J. Numer. Meth. Fluids 68 (10) (2012) 1257–1298.
[14] R. Enright, N. Miljkovic, J. Sprittles, K. Nolan, R. Mitchell, E.N. Wang, How coalescing droplets jump, ACS Nano 8 (10) (2014) 10352–10362.
[15] X. Chen, R.S. Patel, J.A. Weibel, S.V. Garimella, Coalescence-induced jumping of multiple condensate droplets on hierarchical superhydrophobic surfaces, Sci. Rep. 6 (2016) 1–11.
[16] B.J. Briscoe, K.P. Galvin, Growth with coalescence during condensation, Phys. Rev. A 43 (4) (1991) 1906–1917.
[17] R. Narhe, D. Beysens, V.S. Nikolayev, Contact line dynamics in drop coalescence and spreading, Langmuir 20 (4) (2004) 1213–1221.
[18] M. Wu, T. Cubaud, C.M. Ho, Scaling law in liquid drop coalescence driven by surface tension, Phys. Fluids 16 (7) (2004) L51–L54.
[19] K. Rykaczewski, J.H.J. Scott, S. Rajauria, J. Chinn, A.M. Chinn, W. Jones, Three dimensional aspects of droplet coalescence during dropwise condensation on superhydrophobic surfaces, Soft Matter 7 (19) (2011) 8749–8752.
[20] Y. Nam, D. Seo, C. Lee, S. Shin, Droplet coalescence on water repellant surfaces, Soft Matter 11 (1) (2015) 154–160.
[21] M. Sellier, E. Trelluyer, Modeling the coalescence of sessile droplets, Biomicrofluidics 3 (2) (2009) 22412.
[22] D.F. Cooper, B.H. Davey, J.W. Smith, Surface velocities during drop coalescence, Can. J. Chem. Eng. 54 (5) (1976) 631–632.
[23] S.T. Thoroddsen, K. Takehara, T.G. Etoh, The coalescence speed of a pendent and a sessile drop, J. Fluid Mech. 527 (2005) 85–114.
[24] Q. Liao, S.-M. Xing, H. Wang, Experimental investigation on coalescence of liquid drops on homogeneous surface, K Cheng Je Wu Li Hsueh Pao/J. Eng. Thermophys. 27 (2) (2006) 319–321.
[25] F. Mashayek, N. Ashgriz, W.J. Minkowycz, B. Shotorban, Coalescence collision of liquid drops, Int. J. Heat Mass Transf. 46 (1) (2003) 77–89.
[26] M. Mei, B. Yu, M. Zou, L. Luo, A numerical study on growth mechanism of dropwise condensation, Int. J. Heat Mass Transf. 54 (9–10) (2011) 2004–2013.
[27] B.M. Burnside, H.A. Hadi, Digital computer simulation of dropwise condensation from equilibrium droplet to detectable size, Int. J. Heat Mass Transf. 42 (16) (1999) 3137–3146.
[28] L.R. Glicksman, A.W. Hunt, Numerical simulation of dropwise condensation, Int. J. Heat Mass Transf. 15 (11) (1972) 2251–2269.
[29] G.D. Bansal, S. Khandekar, K. Muralidhar, Measurement of heat transfer during drop-wise condensation of water on polyethylene, Nanoscale Microscale Thermophys. Eng. 13 (2009) 184–201.
[30] S.S. Sadhal, W.W. Martin, Heat transfer through using differential drop condensate inequalities, Int. J. Heat Mass Transf. 20 (12) (1977) 1401–1407.
[31] S. Adhikari, M. Nabil, A.S. Rattner, Condensation heat transfer in a sessile droplet at varying Biot number and contact angle, Int. J. Heat Mass Transf. 115 (2017) 926–931.
[32] J.W. Rose, L.R. Glicksman, Dropwise condensation-The distribution of drop sizes, Int. J. Heat Mass Transf. 16 (2) (1973) 411–425.
[33] H.G. Weller, G. Tabor, H. Jasak, C. Fureby, A tensorial approach to computational continuum mechanics using object-oriented techniques, Comput. Phys. 12 (6) (1998) 620–631.
[34] M. Nabil, A.S. Rattner, InterThermalPhaseChangeFoam-A framework for two-phase flow simulations with thermally driven phase change, SoftwareX 5 (2016) 216–226.
[35] A.S. Rattner, S. Garimella, Simple mechanistically consistent formulation for Volume-of-Fluid based computations of condensing flows, J. Heat Transfer 136 (7) (Mar. 2014) 71501.
[36] C.W. Hirt, B.D. Nichols, Volume of Fluid (VOF) methods for the dynamics of free boundaries, J. Comput. Phys. 39 (1) (1981) 201–225.
[37] V.P. Carey, Liquid-Vapor Phase-Change Phenomena, Hemisphere, New York, NY (United States), 2008.
[38] H. Tanaka, T. Tsuruta, A microscopic study of dropwise condensation, Int. J. Heat Mass Transf. 27 (3) (1984) 327–335.
[39] D. Tam, V. von Arnim, G.H. McKinley, A.E. Hosoi, Marangoni convection in droplets on superhydrophobic surfaces, J. Fluid Mech. 624 (2009) 101–123.
[40] J.U. Brackbill, D.B. Kothe, C. Zemach, A continuum method for modeling surface tension, J. Comput. Phys. 100 (2) (1992) 335–354.
[41] K. Yokoi, D. Vadillo, J. Hinch, I. Hutchings, Numerical studies of the influence of the dynamic contact angle on a droplet impacting on a dry surface, Phys. Fluids 21 (7) (2009).
[42] M. Griebel, M. Klitz, Simulation of droplet impact with dynamic contact angle boundary conditions, in: Singular Phenomena and Scaling in Mathematical Models, Springer, Cham, 2014, pp. 297–325.
[43] S. Chavan et al., Heat transfer through a condensate droplet on hydrophobic and nanostructured superhydrophobic surfaces, Langmuir 32 (31) (2016) 7774–7787.
[44] T. Bergman, F. Incropera, D. DeWitt, A. Lavine, Fundamentals of heat and mass transfer, 2011.
[45] S. Adhikari, A.S. Rattner, Heat transfer during condensing droplet coalescence, 2018 [Online]. Available: https://scholarsphere.psu.edu/concern/generic_works/bv73c0509.
[46] "COMSOL, v. 5.2, Stockholm, Sweden." Stockholm.
[47] I.B. Celik, U. Ghia, P.J. Roache, C.J. Freitas, H. Coleman, P.E. Raad, Procedure for estimation and reporting of uncertainty due to discretization in CFD applications, J. Fluids Eng. 130 (7) (2008) 78001.
[48] N. Kapur, P.H. Gaskell, Morphology and dynamics of droplet coalescence on a surface, Phys. Rev. E 75 (5) (2007) 56315.
[49] M. François, Computations of Drop Dynamics with Heat Transfer, University of Florida, 2002.
[50] C.J. Hurst, D.R. Olson, Conduction through droplets during dropwise condensation, J. Heat Transf. 95 (1973) 12–19.
[51] J.L. Mccormick, E. Baer, Developments in Mechanics, Pergamon Press Ltd., 1965.
[52] Y.T. Wu, C.X. Yang, X.G. Yuan, Drop distributions and numerical simulation of dropwise condensation heat transfer, Int. J. Heat Mass Transf. 44 (23) (2001) 4455–4464.